frontiers | Frontiers in Ecology and Evolution

TYPE Original Research
PUBLISHED 10 August 2022
DOI 10.3389/fevo.2022.979194

OPEN ACCESS

EDITED BY
Chuanyu Gao,
Northeast Institute of Geography and Agroecology (CAS), China

REVIEWED BY
Yonghong Xie,
Key Laboratory of Agro-Ecological Processes in Subtropical Region, Institute of Subtropical Agriculture (CAS), China
Junhong Bai,
Beijing Normal University, China

*CORRESPONDENCE
Jisong Yang
yangjisong@ldu.edu.cn
Junbao Yu
yu.junbao@gmail.com

SPECIALTY SECTION
This article was submitted to Conservation and Restoration Ecology, a section of the journal Frontiers in Ecology and Evolution

RECEIVED 27 June 2022
ACCEPTED 08 July 2022
PUBLISHED 10 August 2022

CITATION
Liu X, Sun D, Qin J, Zhang J, Yang Y, Yang J, Wang Z, Zhou D, Li Y, Wang X, Ning K and Yu J (2022) Spatial distribution of soil iron across different plant communities along a hydrological gradient in the Yellow River Estuary wetland. *Front. Ecol. Evol.* 10:979194. doi: 10.3389/fevo.2022.979194

Spatial distribution of soil iron across different plant communities along a hydrological gradient in the Yellow River Estuary wetland

Xue Liu[1], Dandan Sun[1], Jifa Qin[1], Jiapeng Zhang[1], Yunfei Yang[1], Jisong Yang[1,2]*, Zhikang Wang[1], Di Zhou[1], Yunzhao Li[1], Xuehong Wang[1], Kai Ning[2] and Junbao Yu[1]*

[1]The Institute for Advanced Study of Coastal Ecology, Ludong University, Yantai, China, [2]Dongying Academy of Agricultural Sciences, Dongying, China

Iron is an important element and its biogeochemical processes are vital to the matter and energy cycles of wetland ecosystems. Hydrology greatly controls characteristics of soil property and plant community in wetlands, which can regulate the behavior of iron and its oxides. However, it remains unclear how the spatial distribution of iron and its forms in estuarine wetlands responses to hydrological conditions. Five typical plant communities along a naturally hydrological gradient in the Yellow River Estuary wetland, including *Phragmites australis* in freshwater marsh (FPA), *Phragmites australis* in salt marsh (SPA), *Tamarix chinensis* in salt marsh (TC), *Suaeda salsa* in salt marsh (SS) and *Spartina alterniflora* in salt marsh (SA), as sites to collect soil samples. The total iron (Fe_T) and three iron oxides (complexed iron, Fe_p; amorphous iron, Fe_o; free iron, Fe_d) in samples were determined to clarify the spatial distribution of iron and explore its impact factors. The mean contents of Fe_T, Fe_p, Fe_o and Fe_d were 28079.4, 152.0, 617.2 and 8285.3 $mg{\cdot}kg^{-1}$ of soil at 0–40 cm depth in the different sites, respectively. The means were significantly different across communities along the hydrological gradient, with the higher values for SA on the upper intertidal zone and for SPA on the lower intertidal zone, respectively. Iron and its forms were positively correlated with the total organic carbon (TOC), dissolved organic carbon (DOC), total nitrogen (TN) and clay, and negatively correlated with electrical conductivity (EC). The indexes of iron oxides (Fe_p/Fe_d, Fe_o/Fe_d and Fe_d/Fe_T) were also different across communities, with a higher value for SA, which were positively correlated with soil water content (WC) and TOC. The results indicate that a variety of plant community and soil property derived from the difference of hydrology might result in a spatial heterogeneity of iron in estuarine wetlands.

KEYWORDS

iron oxide, spatial distribution, community type, impact factor, estuarine wetland

Introduction

Estuarine wetlands are located in the interaction between water and land ecosystems (Jiang et al., 2006), which are generated by the deposition of sediment carried by rivers into the sea. They play a vital role in maintaining biodiversity, protecting estuarine coastline and regulating climate (Barbier et al., 2011; Jiang et al., 2020). Estuarine wetlands are also one of the important carriers for biogeochemical processes of iron (Fe), sulfur (S), carbon (C), nitrogen (N), phosphorus (P) and so on (Telfeyan et al., 2017; Luo et al., 2019; Lu et al., 2020a). As the fourth abundant element in the earth crust, iron is one of the major redox materials in soil, which is widely distributed in the forms of iron oxide (Weaver and Tarney, 1984). Iron (hydr-)oxides, the main existing forms in soil, are a part of soil colloid, which play an important role in the formation of soil aggregates. The quantities of iron oxides reflect the process and environment of soil-developing (Molina et al., 2001), regulating the nutrient cycles in soil. The redox reaction of iron can affect the decomposition of soil organic matter and the adsorption or transformation of heavy metals in wetland soils (Fimmen et al., 2008; Zhang et al., 2009). Thus, the oxidation/reduction of iron is vital to matter and energy cycles of wetland ecosystems. It's necessary to better understand the importance of iron behaviors for the biogeochemical processes of relevant elements.

Iron oxides in soil consist of the four forms: exchangeable iron, complexed iron (Fe_p), amorphous iron (Fe_o), free iron (Fe_d). Exchangeable iron oxide is abundant in acid soil, while the content in alkaline and neutral soil is less than 1mg kg^{-1}, which is difficult to determine (Zhou and Shen, 2013). Fe_d has a high activity of migration and transformation, and the percentage of Fe_d in Fe_T is called the free degree of iron ($Fe_d/Fe_T \times 100\%$), which can reflect the weathering degree of soil (He and Chen, 1983). Fe_o represents amorphous or weakly crystalline iron oxides, which is one of the most easily utilized forms by plant. As an electron acceptor for iron-reducing microorganisms, it can promote the oxidative decomposition of organic matter (Hori et al., 2010; Yu et al., 2021). The percentage of Fe_o in Fe_d (activation degree: $Fe_o/Fe_d \times 100\%$) can determine the genesis characteristics of soil, reflecting the influence of environment on soil developing. Fe_p belongs to amorphous iron oxides, and its formation process is important for iron ion migration in soil, which is important for the soil fertility (He and Chen, 1983; Tipping et al., 2002). The percentage of Fe_p in Fe_d (complexation degree: $Fe_p/Fe_d \times 100\%$) is important for immobility of soil organic matter. Compared with Fe_p and Fe_d, Fe_o has a large specific surface area, high adsorption and low crystallinity, which is easily utilized by iron-reducing microorganisms and can be reduced quickly (Hyacinthe et al., 2006).

Iron and its oxides in wetland soils can be influenced by biotic and abiotic factors, e.g., hydrological condition, soil property, microbes and vegetation type (Kappler et al., 2004; Zou et al., 2011; Karimian et al., 2018). The redox status in wetland soil depends on hydrological condition, which regulates the oxidation/reduction reaction of iron (Zhang and Furman, 2021). Under reduction conditions, iron exists as dissolved Fe^{2+} and has a strong mobility, while the protection of organic matter can promote the stability of iron complexes; under oxidation conditions, iron can exist as Fe^{3+} and is easily formed to insoluble iron (hydr-)oxides, which would decrease iron migration and transformation in sediments (Melton et al., 2014; Jiang et al., 2019). The pH can affect the redox status, microbial activity and soil adsorption capacity, regulating the transformation and availability of iron in wetland soils (Johnston et al., 2014; Ye et al., 2022). Soil organic matter dynamics is closely related to the biogeochemical cycles of iron, and the reduction rate of Fe(III) will be greatly improved in tidal flat sediments rich in organic matter (Santos-Echeandia et al., 2010; Lalonde et al., 2012). Soil salinity level determines the ionic strength to some extends, which may affect the transformation of iron oxides in salt marshes by regulating the turnover of soil organic carbon and exchange capacity of cations (Williams et al., 1994; Laing et al., 2007; Qu et al., 2018). Due to a high activity of roots, rhizosphere as an important micro-zone in soil is different from the surrounding soil in physical, chemical and biological characteristics, consequently resulting in an acceleration of iron cycles (Adejumo et al., 2018; Zhai et al., 2018).

The Yellow River Estuary wetland is the most complete, broadest and youngest wetland ecosystem in the warm temperate zone of China. There is a naturally hydrological gradient from the riverside to the coast, where various plant communities and soil properties develop on the different micro-topographies. Thus, it is expected to be heterogeneous for soil iron and its forms in the Yellow River Estuary wetland (Zhang et al., 2017). However, it remains unclear how the spatial distribution of iron and its forms in estuarine wetlands responses to hydrological conditions. In the present study, we selected five communities along a hydrological gradient in the Yellow River Estuary wetland to clarify the spatial distribution of iron and explore its impact factors. Our hypotheses are 1) there would be a significantly spatial heterogeneity of iron and its oxides along a hydrological gradient, and 2) the iron distribution could be related to soil property under different hydrological conditions.

Materials and methods

Study area

The Yellow River Estuary wetland (37°40′–38°10′N, 118°41′–119°16′E) is located in the western bank of Bohai Sea. It is an important migration transfer station and winter habitat for birds. The wetland is a flat and wide marine sedimentary plain. The soil is mainly meadow soil and salt marsh soil. The area belongs a warm temperate continental monsoon

and has the climatic characteristics of the same rain-heat season and dry-cold season. The annual average temperature is 12.1°C, and the annual average precipitation is 552.6 mm, most of which is concentrated in summer. The annual average evapotranspiration is 1928.2 mm, which is more threefold than the annual precipitation (Cui et al., 2009). The dominant vegetation types are *P. australis*, *T. chinensis*, *S. salsa*, and *S. alterniflora*, in which *P. australis*, *S. salsa* and *S. alterniflora* are widely distributed.

Study sites and soil sampling

Along a naturally hydrological gradient from the northern side of the Yellow River to the coast, five typical plant communities were selected as sampling sites in turn (**Figure 1**), including *P. australis* in freshwater marsh (FPA), *P. australis* in salt marsh (SPA), *T. chinensis* in salt marsh (TC), *S. salsa* in salt marsh (SS) and *S. alterniflora* in salt marsh (SA), with three repeated samples in each site. The five sites have obviously different hydrological conditions (**Figure 2**). FPA site is located on the riverside of the supratidal zone and is almost unaffected by tides, with sources of river water or/and rainfall and seasonal flooding; SPA site is located on the upper edge of the intertidal zone near the supratidal zone, with a similar hydrological characteristic as FPA, but influenced by extreme tide events; TC site is located on the upper intertidal zone and the surface is occasionally flooded; SS and SA sites are on the middle intertidal zone and the lower intertidal zone, respectively, and the surface is periodic flooded.

In September 2020, soil samples at the depths of 0–10, 10–20, 20–30, and 30–40 cm were collected from the sites using a drill of stainless steel. The subsamples were immediately sealed in an icebox filled N_2 to determine iron oxides. The other subsamples were dried in air to determine soil physicochemical properties, including water content (WC), pH, electrical conductivity (EC), total organic carbon (TOC), dissolved organic carbon (DOC), total nitrogen (TN) and total sulfur (TS). Soil properties were shown in **Table 1**.

Sample measurement

The contents of Fe_T in soil samples were determined using a mothed of phenanthroline - spectrophotometry. Briefly, 0.25 g of dried soil samples were placed in 30 mL polytetrafluoroethylene crucibles and 2–3 drops of water were added to wet samples, followed by addition of 4 mL hydrofluoric acid, 5 mL nitric acid and 0.5 mL perchloric acid. The samples were heated at 300°C until perchlorate acid fumes were thoroughly exhausted. The residues in the crucibles were dissolved with 1 mL hydrochloric acid (1:1), moved into 50 mL colorimetric tubes, colored for 2 h by phenanthroline reagents, and determined the concentrations of Fe_T at 510 nm using the spectrophotometry (TU-1810DS, China).

The Fe_p, Fe_o and Fe_d in the soils were continuously extracted with alkaline sodium pyrophosphate, acid ammonium oxalate and sodium dithionite - sodium citrate - sodium bicarbonate (DCB), respectively (Weiss et al., 2004). Briefly, 1.0 g of wet soil samples and 20 mL 0.1 M sodium pyrophosphate were placed in 50 mL centrifuge tubes under the N_2 condition. After suspension solutions were shocked for 2 h and centrifugated for 10 min, the supernatants were transferred into 50 mL colorimetric tubes, added 5 drops of sulfuric acid (1:1) and 2 drops of 5% potassium permanganate, and kept for a night. The residues were added 40 mL acid ammonium oxalate (0.14 M oxalate acid and 0.2 M ammonium oxalate), shaken in dark for 4 h and centrifugated for 10 min, followed by extracting 5 mL of supernatants. The residues were added 20 mL 1 M sodium citrate and 2.5 mL 1 M sodium bicarbonate, heated for 15 min in water bath at 80°C, and oscillated with addition of 0.5 g sodium hydrosulfite. Then, the suspension solutions were shocked for 2 h and centrifugated for 10 min again, and the supernatants of 5 mL were taken into 50 mL colorimetrical tubes. The extracted solutions of Fe_p, Fe_o, and Fe_d were colored for 24, 12 and 2 h by phenanthroline reagents, respectively, and determined iron concentrations at 510 nm using spectrophotometry.

Iron is calculated as below:

$$Fe_T = \frac{x \times V \times a}{m} \quad (1)$$

$$Fe_y = \frac{x_y \times V \times a \times 1.43}{m} \quad (2)$$

Where Fe_T and Fe_y are content of iron and oxides in the soil ($mg{\cdot}kg^{-1}$), x and x_y are concentrations of iron and oxides in the solution ($mg{\cdot}L^{-1}$), V is volume of the solution (L), a is dilution multiple of the solution, m is weight of dried soil sample (kg) and *1.43* is the coefficient of conversion.

The content of TOC was determined by high-temperature external thermal potassium dichromate oxidation method. The content of DOC was determined by TOC analyzer (Elementar, Germany). The content of TN was determined by continuous flow analyzer (Futura, France). The content of TS was determined by magnesium nitrate oxidation - barium sulfate turbidimetric method. Soil pH (water:soil = 5:1) was determined by pH meter. Soil EC (water:soil = 5:1) was determined by conductivity meter. Soil particle (clay: < 4 μm; silt: 4–63 μm; sand: 64–2,000 μm) was determined by laser particle size analyzer (Mastersizer 3000, England) after pretreatment with hydrogen peroxide and hydrochloric acid.

Statistical analysis

General linear model (GLM) was used to test the effect of community and soil depth on the contents of iron ($p < 0.05$).

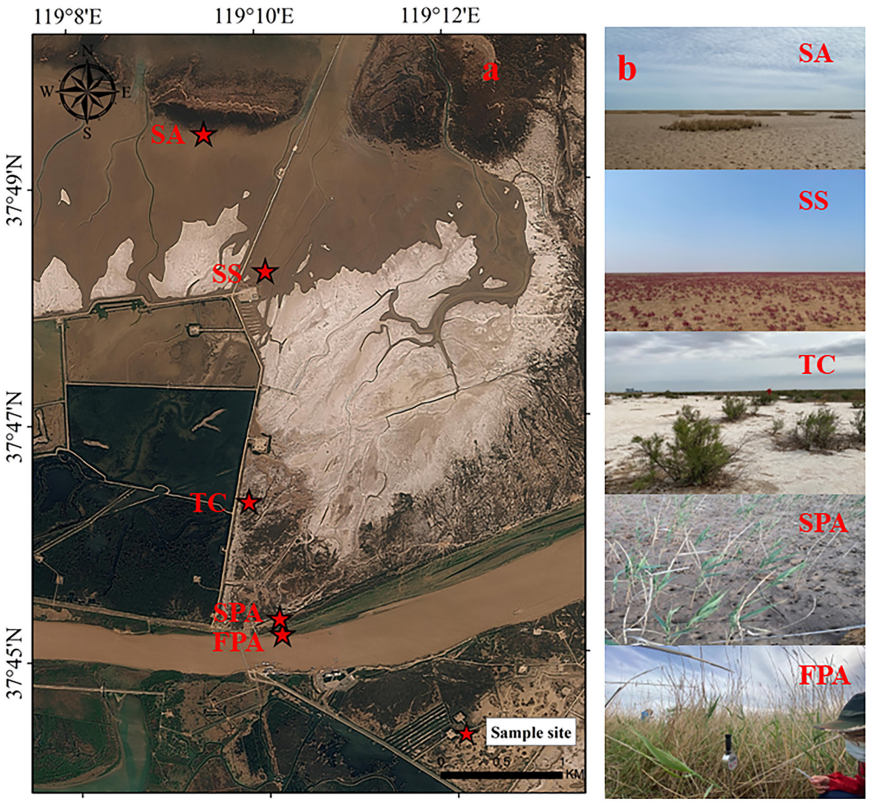

FIGURE 1
The sample sites **(a)** and plant communities **(b)** in the study area. FPA, *P. australis* in freshwater marsh; SPA, *P. australis* in salt marsh; TC, *T. chinensis* in salt marsh; SS, *S. salsa* in salt marsh; SA, *S. alterniflora* in salt marsh.

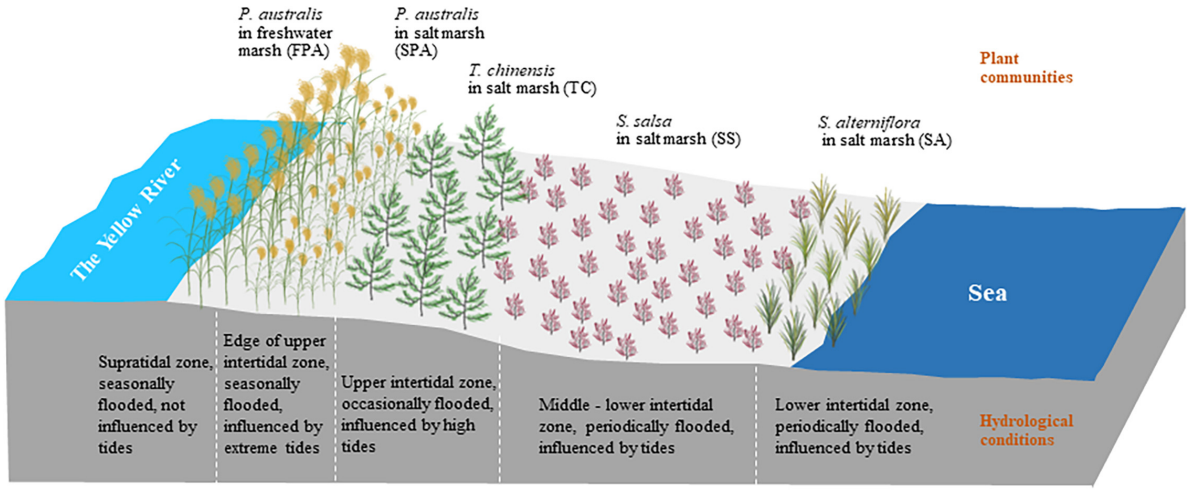

FIGURE 2
Schematic diagram of the hydrological conditions for different plant communities.

TABLE 1 Soil properties in the different communities.

Community type	Soil depth	EC mS·cm^{-1}	WC %	pH	TOC g·kg^{-1}	DOC mg·kg^{-1}	TN g·kg^{-1}	TS mg·kg^{-1}	Clay %
FPA	0–10 cm	0.15 ± 0.021	40.38 ± 0.15	6.41 ± 0.12	3.54 ± 0.21	77.00 ± 24.00	0.32 ± 0.001	79.18 ± 2.91	5.92 ± 0.34
	10–20 cm	0.14 ± 0.042	40.00 ± 1.21	6.60 ± 0.06	3.56 ± 0.13	116.15 ± 1.80	0.32 ± 0.006	91.54 ± 2.91	4.14 ± 0.17
	20–30 cm	0.17 ± 0.007	28.17 ± 3.15	6.73 ± 0.17	3.96 ± 0.11	118.76 ± 27.70	0.32 ± 0.007	93.60 ± 2.91	5.03 ± 0.00
	30–40 cm	0.22 ± 0.014	45.45 ± 3.01	6.73 ± 0.14	3.28 ± 0.07	181.41 ± 9.20	0.38 ± 0.143	212.05 ± 18.94	8.72 ± 0.56
SPA	0–10 cm	1.18 ± 0.050	25.93 ± 0.52	7.24 ± 0.23	10.41 ± 0.39	203.59 ± 7.30	0.44 ± 0.014	679.67 ± 77.20	13.66 ± 044
	10–20 cm	1.30 ± 0.085	26.83 ± 0.63	7.60 ± 0.10	19.58 ± 0.29	366.73 ± 9.20	0.97 ± 0.004	527.23 ± 27.68	16.88 ± 1.08
	20–30 cm	1.77 ± 0.021	48.48 ± 5.12	7.80 ± 0.01	7.53 ± 0.28	170.97 ± 9.20	0.30 ± 0.010	434.53 ± 13.11	13.29 ± 2.14
	30–40 cm	2.00 ± 0.001	37.84 ± 0.78	7.88 ± 0.00	9.45 ± 0.39	198.37 ± 7.40	0.45 ± 0.133	429.38 ± 87.40	25.33 ± 2.35
TC	0–10 cm	9.67 ± 0.849	20.34 ± 1.11	7.80 ± 0.16	5.71 ± 0.04	160.53 ± 5.50	0.28 ± 0.001	853.74 ± 58.27	7.63 ± 0.27
	10–20 cm	6.50 ± 0.092	27.91 ± 0.03	7.85 ± 0.15	5.02 ± 0.11	154.00 ± 11.10	0.29 ± 0.001	476.76 ± 34.96	6.12 ± 0.01
	20–30 cm	3.48 ± 0.001	23.26 ± 0.18	7.77 ± 0.21	3.77 ± 0.11	113.54 ± 1.80	0.30 ± 0.001	405.69 ± 30.59	7.70 ± 0.57
	30–40 cm	3.87 ± 0.001	31.37 ± 0.99	7.93 ± 0.26	5.17 ± 0.14	151.39 ± 7.40	0.29 ± 0.001	541.65 ± 85.94	12.63 ± 0.34
SS	0–10 cm	3.79 ± 0.247	36.96 ± 4.21	8.08 ± 0.01	4.78 ± 0.23	118.76 ± 5.50	0.34 ± 0.069	773.40 ± 40.79	14.71 ± 1.39
	10–20 cm	2.22 ± 0.001	34.21 ± 0.89	8.42 ± 0.13	4.67 ± 0.34	130.51 ± 9.50	0.29 ± 0.002	485.00 ± 2.91	15.41 ± 0.99
	20–30 cm	2.71 ± 0.021	30.43 ± 1.54	8.35 ± 0.13	4.15 ± 0.04	118.76 ± 16.60	0.29 ± 0.005	556.07 ± 85.94	17.29 ± 2.12
	30–40 cm	3.78 ± 0.001	36.84 ± 1.99	8.28 ± 0.14	4.53 ± 0.25	134.42 ± 42.50	0.28 ± 0.002	720.87 ± 129.64	17.12 ± 0.75
SA	0–10 cm	2.99 ± 0.007	48.08 ± 0.68	8.40 ± 0.11	15.19 ± 0.14	191.85 ± 20.30	0.54 ± 0.272	794.00 ± 2.91	20.01 ± 0.01
	10–20 cm	2.35 ± 0.113	39.47 ± 3.65	8.44 ± 0.00	14.01 ± 0.09	168.36 ± 1.80	0.36 ± 0.162	700.27 ± 18.94	17.56 ± 0.33
	20–30 cm	3.47 ± 0.184	48.84 ± 3.10	8.28 ± 0.16	8.18 ± 0.10	151.39 ± 3.70	0.32 ± 0.004	671.43 ± 16.02	23.28 ± 3.01
	30–40 cm	2.97 ± 0.587	51.28 ± 4.01	8.25 ± 0.06	9.83 ± 0.28	261.02 ± 7.40	0.31 ± 0.002	623.02 ± 34.96	19.64 ± 0.95
Differences across communities (0–40 cm)		FPA ^{a}	FPA ^{ab}	FPA ^{a}	FPA ^{a}	FPA ^{a}	FPA ^{ab}	FPA ^{a}	FPA ^{a}
		SPA ^{ab}	SPA ^{bc}	SPA ^{b}	SPA ^{b}	SPA ^{b}	SPA ^{a}	SPA ^{b}	SPA ^{b}
		TC ^{c}	TC ^{c}	TC ^{b}	TC ^{a}	TC ^{a}	TC ^{b}	TC ^{b}	TC ^{a}
		SS ^{b}	SS ^{bc}	SS ^{c}	SS ^{a}	SS ^{a}	SS ^{b}	SS ^{b}	SS ^{b}
		SA ^{b}	SA ^{ad}	SA ^{c}	SA ^{b}	SA ^{ab}	SA ^{ab}	SA ^{b}	SA ^{b}
p		<0.001	0.008	<0.001	0.002	0.027	0.130	<0.001	<0.001

EC, electrical conductivity; WC, water content; TOC, total organic carbon; DOC, dissolved organic carbon; TN, total nitrogen; TS, total sulfur, respectively. The different lower case letters represent a significant difference ($p < 0.05$).

10.3389/fevo.2022.979194

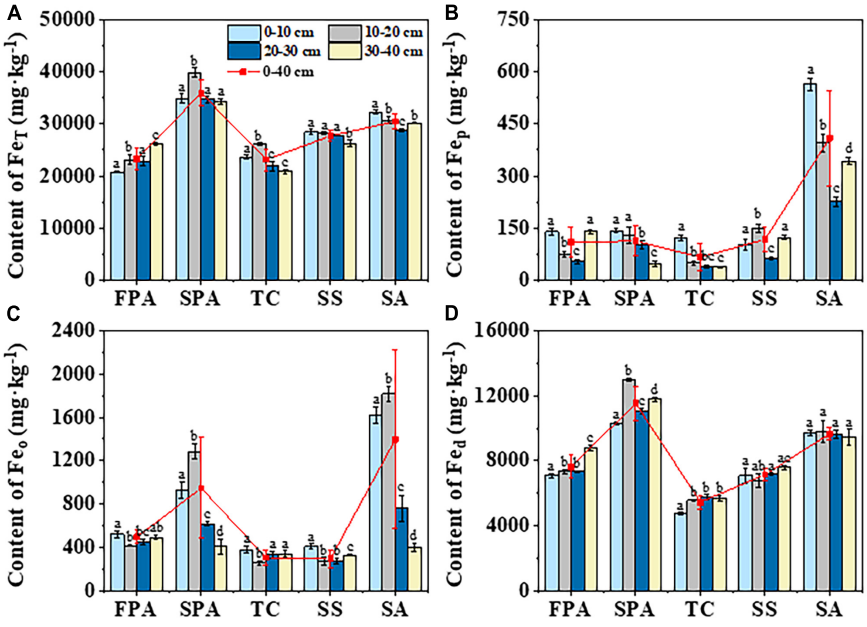

FIGURE 3
Distribution characteristics of Fe_T **(A)**, Fe_p **(B)**, Fe_o **(C)** and Fe_d **(D)** in soils of different communities. Fe_T, total iron; Fe_p, complexed iron; Fe_o, amorphous iron; Fe_d, free iron. Lower letters represent significant differences across depths of the same site ($p < 0.05$).

TABLE 2 Effects of community, soil depth as well as the interaction effects on iron based on general linear model (GLM) at $\alpha = 0.05$.

Item	df		Fe_T	Fe^{2+}	Fe_p	Fe_o	Fe_d	Fe_p/Fe_d	Fe_o/Fe_d	Fe_d/Fe_T
R^2			0.99	0.99	0.99	0.99	0.99	0.99	0.98	0.93
Community type(CT)	4	*F*	1018.9	6882.1	1404.9	617.6	951.2	793.8	317.2	151.4
		p	<0.001	<0.001	<0.001	<0.001	<0.001	<0.001	<0.001	<0.001
Soil depth(SD)	3	*F*	48.1	915.2	247.6	255.6	31.7	264.5	247.1	25.7
		p	<0.001	<0.001	<0.001	<0.001	<0.001	<0.001	<0.001	<0.001
CT × SD	12	*F*	32.4	331.1	75.7	121.8	16.4	52.8	92.0	7.1
		p	<0.001	<0.001	<0.001	<0.001	<0.001	<0.001	<0.001	<0.001

Fe_p, complexed iron; Fe_o, amorphous iron; Fe_d, free iron; Fe_T, total iron, respectively.

The one-way ANOVA with LSD ($p < 0.05$) was used to test the differences in the content of iron and soil depth among the different community types. Origin 2019b was used to determine correlations between the contents of iron and soil properties ($p < 0.05$).

Results

Distribution characteristics of Fe_T in the different communities

The mean contents of Fe_T in soils at 0–40 cm depth across the different communities of FPA, SPA, TC, SS and SA were 23212.0, 35926.4, 23113.4, 27682.3 and 30462.7 mg·kg^{-1}, respectively, with a higher value in SPA and a lower in TC (Figure 3A). There was an increasing trend with soil depth in FPA, a decreasing trend in SS and SA, and a higher value at the 10–20 cm depth in SPA and TC. Overall, the Fe_T contents were significantly different across the different communities (p<0.001) and soil depths (p<0.001) (Table 2).

Distribution characteristics of iron oxides in the different communities

The mean contents of Fe_p, Fe_o and Fe_d ranged from 37.2 to 563.9, from 277.1 to 1814.9 and from 4768.2 to 12986.2 mg·kg^{-1} in soils at 0–40 cm depth across the different communities, respectively (Figures 3B–D). The values were higher in SA or SPA and lower in TC. At the soil depth, the higher values of Fe_p and Fe_o were determined in the upper soil layers (0–10 cm

and 10–20 cm), and the higher value of Fe_d was determined in the lower soil layers (30–40 cm). Overall, there were significant differences across communities ($p < 0.001$) and soil depths ($p<0.001$) (Table 2).

The complexation degree of iron oxide (Fe_p/Fe_d) in soils at 0–40 cm depth across the five communities were 1.3, 0.9, 1.2, 1.5, and 4.0%, respectively, with a higher value in SA and a lower in SS (Figure 4A). The corresponding values for activity degree of iron oxide (Fe_o/Fe_d) were 6.2, 7.0, 6.1, 4.5, and 11.8%, respectively, with a higher value in SA and a lower in SPA (Figure 4B). On the whole, the complexation degree and activity degree of the upper soil layers was higher than that of the lower soil layers. The free degree of iron oxide (Fe_d/Fe_T) were 32.9, 32.1, 23.9, 25.9, and 31.8%, respectively, with a higher value in FPA and a lower in TC (Figure 4C), and the values were higher in the lower soil layers than those in the upper soil layers. Overall, there were significant differences across communities ($p < 0.001$) and soil depths ($p < 0.001$) (Table 2).

Correlations between the contents of iron and soil properties

The mean contents of pH, EC, TOC, DOC, TN, and TS of soil at 0–40 cm depth were 7.74, 2.67 $mS{\cdot}cm^{-1}$, 7.48 $g{\cdot}kg^{-1}$, 167.38 $mg{\cdot}kg^{-1}$, 0.37 $g{\cdot}kg^{-1}$, and 273.66 $mg{\cdot}kg^{-1}$ in FPA, SPA, TC, SS, and SA, respectively (Table 1). The values of pH, EC, TOC, DOC and TS were significantly different across communities ($p < 0.05$). The clay in soils accounted for 4.14–25.33%, which were significantly different across communities ($p < 0.05$).

Fe_T was positively correlated with TOC, DOC, TN, TS, and clay (Figure 5); Fe_p was positively correlated with TOC, WC and clay; Fe_o was positively correlated with TOC, TN, and DOC; Fe_d was positively correlated with TOC, DOC, TN and clay, and negatively correlated with EC. Overall, the contents of iron and its oxides were closely related to organic carbon, nitrogen and soil texture. Fe_p/Fe_d was positively correlated with WC and TOC; Fe_o/Fe_d was positively correlated with TOC; Fe_d/Fe_T was positively correlated with WC, and negatively correlated with EC.

Discussion

Iron and its oxides in wetland soil would be different in regions due to variously environmental and climate conditions (Jiang et al., 2011). The contents of Fe_T in some wetland soils have reported in the previous studies, e.g., 22018.5–27551.9 $mg{\cdot}kg^{-1}$ in mangrove sediment of Manukau Harbour, New Zealand (Bastakoti et al., 2019); 27780–29700 $mg{\cdot}kg^{-1}$ in Jiaozhou Bay coastal wetland, China (Yan et al., 2020); approximately 13067.0 $mg{\cdot}kg^{-1}$ in Sanjiang Plain wetland, China (Huo et al., 2011). In the present study, the means of Fe_T were 20732.3–39879.3 $mg{\cdot}kg^{-1}$ in the Yellow River Estuary wetland soil, with a higher value compared with those in other wetlands. The possible explanation is that the alluvial deposition of sediment carried by the Yellow River leads to the accumulation of abundant iron-bearing minerals in the delta. In the last 70 years, the annual amount of sediment transported from the Yellow River to the Bohai Sea is approximately 6.62×10^8 t (Wang et al., 2021a), and the mean concentration of iron in suspended sediments is 41.3 $mg{\cdot}kg^{-1}$, approximately accounting for 2.7×10^4 t iron transported to sea annually (Yao et al., 2015). Additionally, the Yellow River Delta is a new-born wetland and soil has a lower degree of soil weathering (Fe_d/Fe_T: 20.2–34.3%), which can be beneficial to the enrichment of mineral elements (Liu et al., 2019).

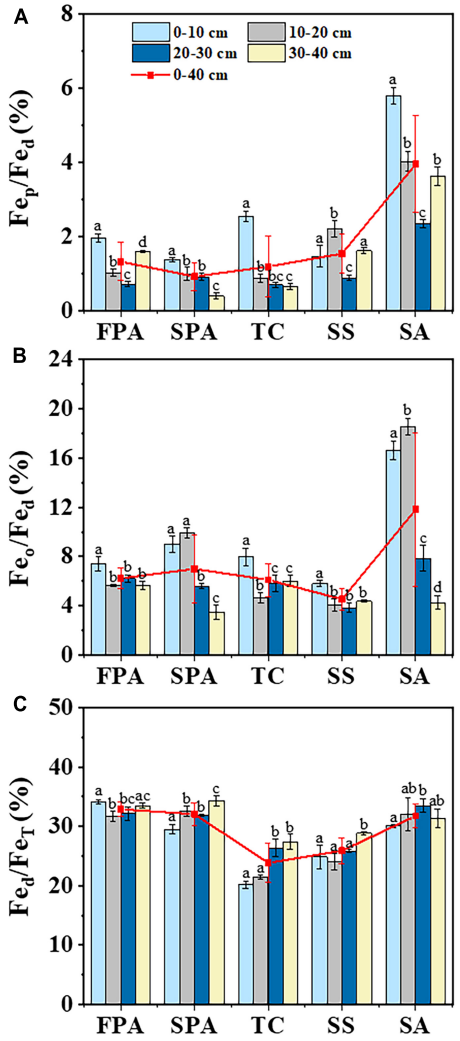

FIGURE 4
Distribution characteristics of iron oxide complexation degree **(A)**, activity degree **(B)** and free degree **(C)** in soils of different communities.

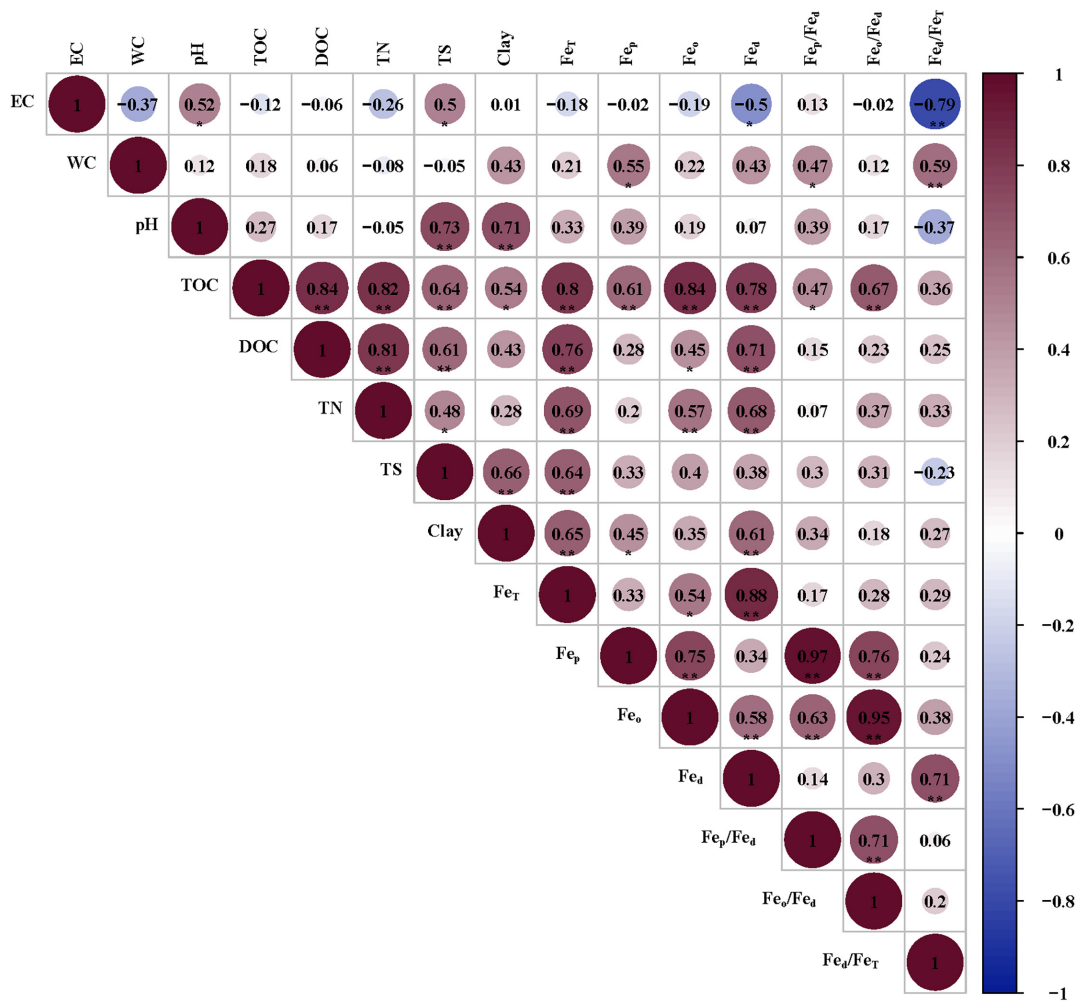

FIGURE 5
Correlations between iron and factors in soils of different communities. EC, WC, TOC, DOC, TN, and TS represent electrical conductivity, water content, total organic carbon, dissolved organic carbon, total nitrogen, total sulfur, respectively. * and ** represent a significant difference at the level of 0.05 and 0.01, respectively.

The distribution of iron and its oxides in wetland soil are controlled by biotic and abiotic factors, such as hydrologic condition, soil properties, vegetation, microbial community and so on (Hoang et al., 2018; Richir et al., 2020; Sui et al., 2021). In the present study, there were significant differences in iron and its oxides across communities. The contents of Fe_T, Fe_o, and Fe_d were higher in SA and SPA, and Fe_p was higher in SA (**Figure 3**), indicating that iron distribution can be controlled by vegetation with different hydrologic conditions. Previous studies demonstrated that hydrologic condition can regulate processes of deposition and transformation in wetlands through changing hydrodynamic and aerobic/anoxic conditions, which would control the stability of organic matter and the immobility of iron ions and oxides in soil (Calabrese and Porporato, 2019; Calabrese et al., 2020). SA is on the lower intertidal zoon and *S. alterniflora* is an invasive plant in the coastal wetland of the Yellow River Estuary, with a total area of 4406.95 hm^2 (Li Y. R. et al., 2021). It develops quickly and has well developed roots (Wan et al., 2014), which can reduce wave erosion and increase sediment accumulation (Wang et al., 2022), resulting in a high input and deposition of iron in the soil. FPA is on the riverside where the sediment carried by floods of the Yellow River deposits, leading to a large amount of iron accumulation. SPA is on the edge of the intertidal zone near the supratidal zone, and the hydrologic condition is only controlled by extreme tide events and river floods, resulting in less frequent and depth of flooding compared with other sites. Iron in soil of SPA might be inclined to form iron (hydr-)oxides (e.g., α-FeOOH, α-Fe_2O_3, γ-FeOOH and γ-Fe_2O_3) and aggravate the enrichment of iron under the weakly anoxic or aerobic environment (Rezapour et al., 2015). Furthermore, plant may be ascribed to the distribution of iron because plant absorption and litter

decomposition can affect iron migration and return into soil (Lu et al., 2020b). The plants of *S. alterniflora* and *P. australis* have a higher biomass (52.59–247.73 $g{\cdot}m^{-2}$ and 5.92–224.46 $g{\cdot}m^{-2}$) (Xie et al., 2021), meaning more iron absorbed by plant and returned into soil as litter decomposition (Costa et al., 2020). In addition, the iron oxides in the rhizosphere can also be regulated by oxygen transported through the plant stress-resistant tissues (Li C. et al., 2021). The well ventilation tissue and root system of *S. alterniflora* and *P. australis* can function as a great ability of radial oxygen loss, which makes iron oxidized to form iron spots in the rhizosphere (Zhang et al., 2019). The spots are mainly composed of amorphous iron and crystalline iron oxides, which can reduce the mobility of iron and promote the enrichment of iron in wetland soil (Wang and Peverly, 1999).

Estuarine wetlands have a stronger carbon sequestration capacity, which is critical for iron immobility and deposition through iron oxides bound on organic carbon (Yu et al., 2019). Dynamics of soil organic carbon is closely related to biogeochemical cycles of iron in wetlands (Lalonde et al., 2012; Wang et al., 2021b). In the present study, total iron and its oxides in soil were positively correlated with TOC and DOC (**Figure 5**), which is consistent to the results reported by some studies in the estuarine wetlands and paddy field (Wang et al., 2012; Sun et al., 2013; Huang et al., 2020). Previous studies have shown that iron oxides can promote the retention of organic carbon in soil through adsorption, chelation or co-precipitation (Duan et al., 2020; Bai et al., 2021). Weak crystalline and amorphous iron oxides have strong adsorption capacity for organic matter, consequently composing stable organic metal complexes (Rezapour et al., 2010). In the study, the contents of Fe_o in SPA and SA were significantly higher than those in the other vegetation types (**Figure 3C**), which corresponded to higher values of TOC and DOC in the sites. Additionally, microbial-mediated iron reduction can significantly affect organic carbon mineralization and thus carbon cycling (Hussain et al., 2019). In the process, organic carbon can provide energy for iron-reducing bacteria, leading to drive the reduction of Fe(III) and promote the migration of iron ions (Lovley, 1997; Xiao et al., 2019).

The biogeochemical processes of iron in coastal wetland soil can be coupled with nitrogen cycles through surface adsorption of iron oxides and Fe(III) reduction (Zhao et al., 2019). In the present study, Fe_o, Fe_d and Fe_T were positively correlated with TN (**Figure 5**). In the Yellow River Estuary wetland, inorganic nitrogen accounted for less than 20% of the total nitrogen (Mu et al., 2012). Iron oxides can promote the stability of organic nitrogen and inhibit the nitrogen mineralization by adsorbing organic matter on the surface (Heng et al., 2010; Liu et al., 2020). However, the microbial reduction of Fe(III) plays an important regulation in the transformation nitrogen. Guan et al. (2018) found that adding Fe(III) oxide has increased N_2 production of sediments in the mangrove wetland, suggesting that Fe(III) reduction could promote anaerobic ammonia oxidation and increase nitrogen loss. The result about the positive correlation between iron oxides and TN in our study indicates that surface adsorption of iron oxides but Fe(III) reduction may contribute nitrogen fixation. Moreover, the biogeochemical processes of iron are also closely related with sulfur cycles in coastal wetlands (Burton et al., 2011). In the present study, we found that Fe_T was significantly positively correlated with TS (**Figure 5**). In the coastal wetlands, H_2S can act as a reducing agent for Fe(III) oxides in sulfide-rich environments (Johnston et al., 2014; Sheng et al., 2015; Karimian et al., 2018), and sulfide (S^{2-}) reacts with Fe^{2+} to form FeS or FeS_2 in the process of sulfate reduction, which could promote iron immobility in the sediment (Schoepfer et al., 2014; Hu et al., 2022). *S. alterniflora* is on the lower tide zone with a higher sulfur content in soil (**Table 1**), possibly ascribed to a higher content of iron oxides due to more iron combining with sulfur to form pyrite. However, FPA is in the freshwater environment with a lower content of sulfur in soil, which may cause less iron combined by sulfur, possibly resulting in more iron loss in the form of dissolved Fe^{2+} and more iron oxides remained in soil.

Soil texture is one of the important factors affecting iron forms, and especially clay can promote the enrichment of iron (Finck, 2020). We found that the contents of soil clay in the Yellow River Estuary wetland ranged from 4.14 to 25.33% (**Table 1**), which were positively correlated with Fe_T, Fe_d and Fe_p (**Figure 5**). Clay minerals can be wrapped by Fe/Al oxides to form stable aggregate structure to improve water retention capacity and physical quality of soil (AL-Shamare and Essa, 2021; Bai et al., 2021; Mendes et al., 2022). Moreover, clay minerals can also be combined with soil organic matter to form organic-inorganic complex, leading to a stronger immobility of iron (Zhang et al., 2001; Angst et al., 2021). The salinity reflects the ionic strength in soil and has an important impact on soil properties and the distribution of iron and its oxides (Celik et al., 2021; Ury et al., 2022). Previous studies showed that iron from boreal rivers display a higher resistance toward salinity-induced aggregation, e.g., iron (hydr-)oxides are selectively removed by aggregation processes, and organic iron complexes are less affected by increasing salinity (Herzog et al., 2019). In the present study, iron contents were negatively correlated with EC to some extents (**Figure 5**). Besides FPA, the other four communities were influenced by tides in different intensity (**Figure 2**), and the hydrologic conditions varied with the depth and frequency of tidal flood. Therefore, soil EC in the communities showed a great variety, which may contribute the differentiation of iron oxides in soils. For example, the soil surface in TC was always exposed and submerged only at high tides, which leads to the salt accumulation in soil due to an intense evaporation/transpiration. Consequently, the iron oxides are relatively low under the action of salinity aggregation. However, there was no obviously negative effect of salinity on iron content in FPA, which indicated that the distribution of iron and its oxides in the coastal wetland

soils could be controlled by the interaction of factors. In addition, salinity of coastal wetland soil has an important effect on microbial community and activity by regulating soil extracellular osmotic potential, which can directly or indirectly regulate the transformation and bioavailability of iron (Richard and Frances, 2001; Laing et al., 2007).

The values of Fe_d/Fe_T, Fe_o/Fe_d and Fe_p/Fe_d are important indexes which can indicate the degree of soil weathering, which is controlled by environmental conditions (He and Chen, 1983). We found that all the three degrees were different across the communities, with a higher value in the *S. alterniflora* and *P. australis* communities (**Figure 4** and **Table 2**), indicating a well weathering for the soils. In the present study, the values of Fe_d/Fe_T in different communities were negatively correlated with EC and positively correlated with WC, which possibly ascribed to the negatively effects of EC and the positively effects of WC on iron oxides, respectively (**Figure 5**). The values of Fe_p/Fe_d and Fe_o/Fe_d were positively correlated with TOC (**Figure 5**). Organic matter is rich in fulvic acid which can inhibit iron oxides deposition, and thus increases the activation degree of iron oxides (Fan et al., 2016). Free iron oxides are effective adsorbents for multivalence superoxide anions; of them, amorphous iron has a higher affinity for multivalence superoxide anions due to a large specific surface area and a high reactivity of surface functional groups, which has a stronger ability to combined soil organic matter (Zhao et al., 2018). Moreover, free iron oxides are also an important mineral cement in soil, and their decrease may lead to the deterioration of soil structure and aggravate the degradation of soil (Duiker et al., 2003; Zhang et al., 2016). Therefore, free iron oxides can regulate carbon sequestration because they can be combined with organic matter through adsorption/coprecipitation to form a stable Fe-OC complex (Zhang et al., 2012; Zhao et al., 2017). Given that hydrological conditions in the estuarine wetlands would alter with climate change, the iron and its forms could shift accordingly. The result suggests that the carbon sequestration in estuarine wetlands could change with hydrological alteration under climate change.

Conclusion

In the study, we found that iron and its forms in estuarine wetland soils varied with communities along a hydrological gradient. The contents of iron and its oxides were higher in the *S. alterniflora* and *P. australis* (in the salt marsh) communities, which was positively correlated with soil organic carbon, nitrogen and clay, and negatively correlated with salinity. The weathering indicators were also different across plant communities with a higher free degree in *S. alterniflora* and *P. australis* communities, which was correlated with soil water content, organic matter and salinity. The results indicate that iron and its forms in estuarine wetland soils depends on hydrological conditions, suggesting that high strength of hydrological effects (e.g., frequency and depth of tides or floods) may benefit the iron immobility. The results would be helpful to understand the mechanisms of iron biogeochemistry and explore the coupled cycles of iron with other elements in estuarine wetlands.

Data availability statement

The original contributions presented in this study are included in the article/supplementary material, further inquiries can be directed to the corresponding authors.

Author contributions

XL: methodology, validation, and writing – original draft. DS, JQ, JZ, YY, YL, and XW: resources and investigation. JSY: conceptualization, supervision, and writing – review and editing. ZW, DZ, and KN: software and data curation. JBY: formal analysis and validation. All authors contributed to the article and approved the submitted version.

Funding

This work was supported by the National Natural Science Foundation of China (41871087, U1806218, and 42171111), Yellow River Delta Scholar Talent Project, and the Project of the Cultivation Plan of Superior Discipline Talent Teams of Universities in Shandong Province "The Coastal Resources and Environment Team for Blue-Yellow Area".

Conflict of interest

The authors declare that the research was conducted in the absence of any commercial or financial relationships that could be construed as a potential conflict of interest.

Publisher's note

References

Adejumo, S. A., Tiwari, S., Shinde, V., and Sarangi, B. K. (2018). Heavy metal (Pb) accumulation in metallophytes as influenced by the variations in rhizospheric and non-rhizospheric soils physico-chemical characteristics. *Int. J. Phytoremediation* 20, 237–248. doi: 10.1080/15226514.2017.1374333

AL-Shamare, A. H., and Essa, S. K. (2021). Contribution of clay, silt, organic matter, free iron oxides and active calcium carbonate in cation wxchange capacity in Wasit and Maysan Soils. *Indian J. Ecol.* 48, 61–65.

Angst, G., Pokorn, J., Mueller, C. W., Prater, I., Preusser, S., Kandeler, E., et al. (2021). Soil texture affects the coupling of litter decomposition and soil organic matter formation. *Soil Biol. Biochem.* 159:108302. doi: 10.1016/j.soilbio.2021.108302

Bai, J., Luo, M., Yang, Y., Xiao, S. Y., Zhai, Z. F., and Huang, J. F. (2021). Iron-bound carbon increases along a freshwater-oligohaline gradient in a subtropical tidal wetland. *Soil Biol. Biochem.* 154:108128. doi: 10.1016/j.soilbio.2020.108128

Barbier, E. B., Hacker, S. D., Koch, E. W., Stier, A. C., and Silliman, B. R. (2011). "Estuarine and coastal ecosystems and their services". *Treatise on Estuarine and Coastal Science*, eds E. Wolanski and D. McLusky (Amsterdam: Elsevier Science) 12, 109–127. doi: 10.1016/B978-0-12-374711-2.01206-7

Bastakoti, U., Bourgeois, C., Marchand, C., and Alfaro, A. C. (2019). Urban-rural gradients in the distribution of trace metals in sediments within temperate mangroves (New Zealand). *Mar. Pollut. Bull.* 149:110614. doi: 10.1016/j.marpolbul.2019.110614

Burton, E. D., Bush, R. T., Johnston, S. G., Sullivan, L. A., and Keene, A. F. (2011). Sulfur biogeochemical cycling and novel Fe-S mineralization pathways in a tidally re-flooded wetland. *Geochim. Cosmochim. Acta.* 75, 3434–3451. doi: 10.1016/j.gca.2011.03.020

Calabrese, S., and Porporato, A. (2019). Impact of ecohydrological fluctuations on iron-redox cycling. *Soil Biol. Biochem.* 133, 188–195. doi: 10.1016/j.soilbio.2019.03.013

Calabrese, S., Barcellos, D., Thompson, A. A., and Porporato, A. (2020). Theoretical constraints on Fe reduction rates in upland soils as a function of hydroclimatic conditions. *J. Geophys. Res.* 125, e2020JG005894 doi: 10.1029/2020JG005894

Celik, S., Anderson, C. J., Kalin, L., and Rezaeianzadeh, M. (2021). Long-term salinity, hydrology, and forested wetlands along a tidal freshwater gradient. *Estuaries Coast.* 44, 1816–1830. doi: 10.1007/s12237-021-00911-8

Costa, L., Mirlean, N., Quintana, G., Adebayo, S., and Johannesson, K. (2020). Effects of bioirrigation and salinity on arsenic distributions in ferruginous concretions from salt marsh dediment cores (Southern Brazil). *Aquat. Geochem.* 27, 79–103. doi: 10.1007/s10498-020-09387-7

Cui, B. S., Yang, Q. C., Yang, Z. F., and Zhang, K. J. (2009). Evaluating the ecological performance of wetland restoration in the Yellow River Delta. China. *Ecol. Eng.* 35, 1090–1103. doi: 10.1016/j.ecoleng.2009.03.022

Duan, X., Yu, X. F., Li, Z., Wang, Q. G., Liu, Z. P., and Zou, Y. C. (2020). Iron-bound organic carbon is conserved in the rhizosphere soil of freshwater wetlands. *Soil Biol. Biochem.* 149:107949. doi: 10.1016/j.soilbio.2020.107949

Duiker, S. W., Rhoton, F. E., Torrent, J., Smeck, N. E., and Lal, R. (2003). Iron (hydr) oxide crystallinity effects on soil aggregation. *Soil Sci. Soc. Am. J.* 67, 606–611. doi: 10.2136/sssaj2003.6060

Fan, S. S., Chang, F. H., Hsueh, H. T., and Ko, T. H. (2016). Measurement of total free iron in soils by H_2S chemisorption and comparison with the citrate bicarbonate dithionite method. *J. Anal. Methods Chem.* 2016:7213542. doi: 10.1155/2016/7213542

Fimmen, R. L., Richter, D. D., Vasudevan, D., Williams, M. A., and West, L. T. (2008). Rhizogenic Fe-C redox cycling: a hypothetical biogeochemical mechanism that drives crustal weathering in upland soils. *Biogeochemistry* 87, 127–141. doi: 10.1007/s10533-007-9172-5

Finck, N. (2020). Iron speciation in Opalinus clay minerals. *Appl. Clay Sci.* 193:105679. doi: 10.1016/j.clay.2020.105679

Guan, Q. S., Cao, W. Z., Wang, M., Wu, G. J., Wang, F. F., Jiang, C., et al. (2018). Nitrogen loss through anaerobic ammonium oxidation coupled with iron reduction in a mangrove wetland. *Eur. J. Soil Sci.* 69, 732–741. doi: 10.1111/ejss.12552

He, Q., and Chen, J. F. (1983). Determination of free and complexed iron in soil. *Soil* 15, 242–245. doi: 10.13758/j.cnki.tr.1998.01.001

Heng, L. S., Wang, D. C., Jiang, X., Rao, W., Zhang, W. H., Guo, C. Y., et al. (2010). Relationship between Fe. Al oxides and stable organic carbon, nitrogen in the Yellow-Brown Soils. *Environ. Sci.* 31, 2748–55. doi: 10.13227/j.hjkx.2010.11.040

Herzog, S. D., Conrad, S., Ingri, J., Persson, P., and Kritzberg, E. S. (2019). Spring flood induced shifts in Fe speciation and fate at increased salinity. *Appl. Geochem.* 109:104385. doi: 10.1016/j.apgeochem.2019.104385

Hoang, T. K., Probst, A., Orange, D., Gilbert, F., Elger, A., Kallerhoff, J., et al. (2018). Bioturbation effects on bioaccumulation of cadmium in the wetland plant Typha latifolia: a nature-based experiment. *Sci. Total Environ.* 618, 1284–1297. doi: 10.1016/j.scitotenv.2017.09.237

Hori, T., Müller, A., Igarashi, Y., Conrad, R., and Friedrich, M. W. (2010). Identification of iron-reducing microorganisms in anoxic rice paddy soil by ^{13}C-acetate probing. *ISME J.* 4, 267–278. doi: 10.1038/ismej.2009.100

Hu, M. J., Sardans, J., Le, Y. X., Yan, R. B., Zhong, Y., and Peñuelas, J. (2022). Effects of wetland types on dynamics and couplings of labile phosphorus, iron and sulfur in coastal wetlands during growing season. *Sci. Total Environ.* 830:154460. doi: 10.1016/j.scitotenv.2022.154460

Huang, X. L., Kang, W. J., Wang, L., Yu, G. H., Ran, W., Hong, J. P., et al. (2020). Preservation of organic carbon promoted by iron redox transformation in a rice-wheat cropping system. *Appl. Soil Ecol.* 147:103425. doi: 10.1016/j.apsoil.2019.103425

Huo, L. L., Lv, X. G., and Zou, Y. C. (2011). Changes of iron in top soil of paddies as affected by reclamation ages in Sanjiang Plain. *Bull. Soil Water Conserv.* 31:5. doi: 10.1016/S1671-2927(11)60313-1

Hussain, S., Zhang, M., Zhu, X. X., Khan, M. H., Li, L. F., and Cao, H. (2019). Significance of Fe(II) and environmental factors on carbon-fixing bacterial community in two paddy soils. *Ecotoxicol. Environ. Saf.* 182:109456. doi: 10.1016/j.ecoenv.2019.109456

Hyacinthe, C., Bonneville, S., and Cappellen, P. V. (2006). Reactive iron(III) in sediments: chemical versus microbial extractions. *Geochim. Cosmochim. Acta* 70, 4166–4180. doi: 10.1016/j.gca.2006.05.018

Jiang, M., Lu, X. G., Wang, H. Q., Zou, Y. C., and Wu, H. T. (2011). Transfer and transformation of soil iron and implications for hydrogeomorpholocial changes in Naoli River catchment. Sanjiang Plain, northeast China. *Chin. Geogr. Sci.* 21, 149–158. doi: 10.1007/s11769-011-0454-4

Jiang, M., Lv, X. G., Yang, Q., and Tong, S. Z. (2006). Iron biogeochemical cycle and its environmental effect in wetlands. *Acta Pedologica Sinica* 3, 493–499. doi: 10.11766/trxb200412270320

Jiang, X., Zhu, L., Xu, S. G., and Xie, Z. G. (2019). Institute of water and environmental research, faculty of infra effects of seasonal stratification and suspended sediment behaviors on the mobilization of manganese and iron in a drinking water reservoir-a case of Biliuhe reservoir, Liaoning province. *Lake Sci.* 375–385. doi: 10.18307/2019.0207

Jiang, Y. X., Wang, Y. Z., Zhou, D. M., Ke, Y. H., Bai, J. H., Li, W. W., et al. (2020). The impact assessment of hydro-biological connectivity changes on the estuary wetland through the ecological restoration project in the Yellow River Delta. China. *Sci. Total Environ.* 758:143706. doi: 10.1016/j.scitotenv.2020.143706

Johnston, S. G., Burton, E. D., Aaso, T., and Tuckerman, G. (2014). Sulfur, iron and carbon cycling following hydrological restoration of acidic freshwater wetlands. *Chem. Geol.* 371, 9–26. doi: 10.1016/j.chemgeo.2014.02.001

Kappler, A., Benz, M., Schink, B., and Brune, A. (2004). Electron shuttling via humic acids in microbial iron(III) reduction in a freshwater sediment. *FEMS Microbiol. Ecol.* 47, 85–92. doi: 10.1016/S0168-6496(03)00245-9

Karimian, N., Johnston, S. G., and Burton, E. D. (2018). Iron and sulfur cycling in acid sulfate soil wetlands under dynamic redox conditions: a review. *Chemosphere* 197, 803–816. doi: 10.1016/j.chemosphere.2018.01.096

Laing, G. D., Vandecasteele, B., Grauwe, P. D., Moors, W., Lesage, E., Meers, E., et al. (2007). Factors affecting metal concentrations in the upper sediment layer of intertidal reedbeds along the river Scheldt. *J. Environ. Monitor.* 9, 449–455. doi: 10.1039/b618772b

Lalonde, K., Mucci, A., Ouellet, A., and Gélinas, Y. (2012). Preservation of organic matter in sediments promoted by iron. *Nature* 483, 198–200. doi: 10.1038/nature10855

Li, C., Ding, S. M., Ma, X., Chen, M. S., Zhong, Z. L., Zhang, Y., et al. (2021). O_2 distribution and dynamics in the rhizosphere of *Phragmites australis*, and implications for nutrient removal in sediments. *Environ. Poll.* 287:117193. doi: 10.1016/j.envpol.2021.117193

Li, Y. R., Wu, H. T., Zhang, S., Lu, X., and Lu, K. L. (2021). Morphological characteristics and changes of tidal creeks in coastal wetlands of the Yellow River Delta under *spartina alterniflora* invasion and continuous expansion. *Wetl. Sci.* 19, 88–97. doi: 10.13248/j.cnki.wetlandsci.2021.01.009

Liu, C. F., Wang, W. X., and Ma, H. L. (2020). Role of Fe and Al oxides in soil nitrogen transformation under nitrogen addition condition. *Res. Environ. Sci.* 1946–1953. doi: 10.13198/j.issn.1001-6929.2019.12.03

Liu, F. D., Zheng, B. W., Zheng, Y., Mo, X., and Li, D. (2019). Accumulation risk and sources of heavy metals in supratidal wetlands along the west coast of the Bohai Sea. *RSC Adv.* 9, 30615–30627. doi: 10.1039/C9RA05332H

Lovley, D. R. M. (1997). Microbial Fe(III) reduction in subsurface environments. *FEMS Microbiol. Rev.* 20, 305–313.

Lu, Q. Q., Bai, J. H., Yan, D. H., Cui, B. S., and Wu, J. J. (2020a). Sulfur forms in wetland soils with different flooding periods before and after flow-sediment regulation in the Yellow River Delta. China. *J. Clean. Prod.* 276:122969. doi: 10.1016/j.jclepro.2020.122969

Lu, Q. Y., Pei, L. X., Ye, S. Y., Laws, E. A., and Brix, H. (2020b). Negative feedback by vegetation on soil organic matter decomposition in a coastal wetland. *Wetlands* 40, 2785–2797. doi: 10.1007/s13157-020-01350-0

Luo, M., Zhu, W. F., Huang, J. F., Liu, Y. X., Duan, X., Wu, J., et al. (2019). Anaerobic organic carbon mineralization in tidal wetlands along a low-level salinity gradient of a subtropical estuary: rates, pathways, and controls. *Geoderma* 33, 1245–1257. doi: 10.1016/j.geoderma.2018.07.030

Melton, E. D., Swanner, E. D., Behrens, S., Schmidt, C., and Kappler, K. A. (2014). The interplay of microbially mediated and abiotic reactions in the biogeochemical Fe cycle. *Nat. Rev. Microbiol.* 12, 797–808. doi: 10.1038/nrmicro3347

Mendes, W. D. S., Demattê, J. A. M., Minasny, B., Silvero, N. E. Q., Bonfatti, B. R., and Safanelli, J. L. (2022). Free iron oxide content in tropical soils predicted by integrative digital mapping. *Soil Tillage Res.* 219:105346. doi: 10.1016/j.still.2022.105346

Molina, N. C., Caceres, M. R., and Pietroboni, A. M. (2001). Factors affecting aggregate stability and water dispersible clay of recently cultivated semiarid soils of Argentina. *Arid Land Res. Manag.* 15, 77–87. doi: 10.1080/153249801300000833

Mu, X. J., Sun, Z. G., and Liu, X. T. (2012). Spatial distribution patterns of nitrate nitrogen and ammonia nitrogen in typical tidal marsh soils of Yellow River Delta. *Bull. Soil Water Conserv.* 32, 256–261. doi: 10.13961/j.cnki.stbctb.2012.06.005

Qu, W. D., Li, J. Y., Han, G. X., Wu, H. T., Song, W. M., and Zhang, X. S. (2018). Effect of salinity on the decomposition of soil organic carbon in a tidal wetland. *J. Soils Sediments* 19, 609–617. doi: 10.1007/s11368-018-2096-y

Rezapour, S., Azhah, H., Momtaz, H., and Ghaemian, N. (2015). Changes in forms and distribution pattern of soil iron oxides due to long-term cropping in the Northwest of Iran. *Environ. Earth Sci.* 73, 7275–7286.

Rezapour, S., Jafarzadeh, A. A., Samadi, A., and Oustan, S. (2010). Distribution of iron oxides forms on a transect of calcareous soils, north-west of Iran. *Arch. Agron. Soil Sci.* 56, 165–182. doi: 10.1038/ismej.2014.77

Richard, R. G., and Frances, R. P. (2001). Changes in dissolved and total Fe and Mn in a young constructed wetland: implications for retention performance. *Ecol. Eng.* 17, 373–384. doi: 10.1016/j.biocon.2015.11.019

Richir, J., Bouillon, S., Gobert, S., Skov, M. W., and Borges, A. V. (2020). Editorial: structure, functioning and conservation of coastal vegetated wetlands. *Front. Ecol. Evol.* 8:134. doi: 10.3389/fevo.2020.00134

Santos-Echeandia, J., Vale, C., Caetano, M., Pereira, P., and Prego, R. (2010). Effect of tidal flooding on metal distribution in pore waters of marsh sediments and its transport to water column (Tagus estuary. Portugal). *Mar. Environ. Res.* 70, 358–367. doi: 10.1016/j.marenvres.2010.07.003

Schoepfer, V. A., Bernhardt, E. S., and Burgin, A. J. (2014). Iron clad wetlands: soil iron-sulfur buffering determines coastal wetland response to salt water incursion. *Biogeosciences* 119, 2209–2219. doi: 10.1002/2014JG002739

Sheng, Y. G., Sun, Q. Y., Shi, W. J., Bottrell, S., and Mortimer, R. (2015). Geochemistry of reduced inorganic sulfur, reactive iron, and organic carbon in fluvial and marine surface sediment in the Laizhou Bay region. China. *Environ. Earth Sci.* 74, 1151–1160. doi: 10.1007/s12665-015-4101-8

Sui, X., Zhang, R. G., Frey, B., Yang, L. B., Liu, Y. N., Ni, H. W., et al. (2021). Soil physicochemical properties drive the variation in soil microbial communities along a forest successional series in a degraded wetland in northeastern China. *Ecol. Evol.* 11, 2194–2208. doi: 10.1002/ece3.7184

Sun, W. G., Gan, Z. T., Sun, Z. G., Li, L. L., Sun, J. K., Sun, W. L., et al. (2013). Spatial distribution characteristics of Fe and Mn contents in the new-born coastal marshes in the Yellow River Estuary. *Environ. Sci.* 34, 4411–4419. doi: 10.13227/j.hjkx.2013.11.045

Telfeyan, K., Breaux, A., Kim, J., Cable, J. E., Kolker, A. S., Grimm, D. A., et al. (2017). Arsenic, vanadium, iron, and manganese biogeochemistry in a deltaic wetland, southern Louisiana. USA. *Mar. Chem.* 192, 32–48. doi: 10.1016/j.marchem.2017.03.010

Tipping, E., Rey-Castro, C., Bryan, S. E., and Hamilton-Taylor, J. (2002). Al(III) and Fe(III) binding by humic substances in freshwaters, and implications for trace metal speciation. *Geochim. Cosmochim. Acta* 66, 3211–3224. doi: 10.1016/S0016-7037(02)00930-4

Ury, E. A., Wright, J. P., Ardón, M., and Bernhardt, E. S. (2022). Saltwater intrusion in context: soil factors regulate impacts of salinity on soil carbon cycling. *Biogeochemistry* 157, 215–226. doi: 10.1007/s10533-021-00869-6

Wan, H. W., Qiao, W., Jiang, D., Fu, J. Y., Yang, Y. P., and Liu, X. M. (2014). Monitoring the invasion of *Spartina Alterniflora* using very high resolution unmanned aerial vehicle imagery in Beihai. Guangxi (China). *Sci. World J.* 2014:638296. doi: 10.1155/2014/638296

Wang, B., Zhang, K., Liu, Q. X., He, Q., van de Koppel, J., Teng, S. N., et al. (2022). Long-distance facilitation of coastal ecosystem structure and resilience. *PNAS* 119:e2123274119. doi: 10.1073/pnas.2123274119

Wang, J. J., Bing, S., and Hu, Y. Z. (2021a). Prediction of sediment transport from the Yellow River to the Bohai Sea based on the CEEMDAN-WNN coupled model. *Trans. Oceanol. Limnol.* 43, 34–41. doi: 10.13984/j.cnki.cn27-1141.2021.05.005

Wang, S. M., Jia, Y. F., Liu, T., Wang, Y. Y., Liu, Z. G., and Feng, X. J. (2021b). Delineating the role of calcium in the large-scale distribution of metal-bound organic carbon in soils. *Geophys. Res. Lett.* 48:e2021GL092391. doi: 10.1029/2021GL092391

Wang, T. G., and Peverly, J. H. (1999). Iron oxidation states on root surfaces of a wetland plant (*phragmites australis*). *Soil Sci. Soc. Am. J.* 63, 247–252. doi: 10.2136/sssaj1999.03615995006300010036x

Wang, W. Q., Wang, C., Zeng, C. S., and Tong, C. (2012). Soil carbon, nitrogen and phosphorus ecological stoichiometry of *Phragmites australis* wetlands in different reaches in Minjiang River estuary. *Acta Ecol. Sinica* 32, 4087–4093. doi: 10.5846/stxb201106160817

Weaver, B. L., and Tarney, J. (1984). Empirical approach to estimating the composition of the continental crust. *Nature* 310, 575–577. doi: 10.1038/310575a0

Weiss, J. V., Emerson, D., and Megonigal, J. P. (2004). Geochemical control of microbial Fe(III) reduction potential in wetlands: comparison of the rhizosphere to non-rhizosphere soil. *FEMS Microbiol. Ecol.* 48, 89–100. doi: 10.1016/j.femsec.2003.12.014

Williams, T. P., Bubb, J. M., and Lester, J. N. (1994). Metal accumulation within salt marsh environments: a review. *Mar Pollut. Bull.* 28, 277–290. doi: 10.1016/0025-326X(94)90152-X

Xiao, D. R., Lei, D., Kim, D. G., Huang, C. B., and Tian, K. (2019). Carbon budgets of wetland ecosystems in China. *Glob. Change Biol.* 25, 2061–2076. doi: 10.1111/gcb.14621

Xie, X., Li, X. W., Bai, J. H., and Zhi, L. H. (2021). Variations of aboveground biomass of 4 kinds of Typical Plants with surface elevation of wetlands in the Yellow River Delta. *Wetl. Sci.* 19, 226–231. doi: 10.13248/j.cnki.wetlandsci.2021.02.010

Yan, Q., Xie, W. X., Sha, M. Q., and Li, P. (2020). Effects of *spartina alterniflora* invasion on soil total iron distribution in estuary wetland of Jiaozhou Bay. *Acta Ecol. Sinica* 40, 3991–3999. doi: 10.5846/stxb201903120466

Yao, Q. Z., Wang, X. J., Jian, H. M., Chen, H. T., and Yu, Z. G. (2015). Characterization of the particle size fraction associated with heavy metals in suspended sediments of the Yellow River. *Int. J. Environ. Res. Public Health* 12, 6725–6744. doi: 10.3390/ijerph120606725

Ye, C. L., Huang, W. J., Hall, S. J., and Hu, S. J. (2022). Association of organic carbon with reactive iron oxides driven by soil pH at the global scale. *Glob. Biogeochem. Cycles* 36:e2021GB007128. doi: 10.1029/2021GB007128

Yu, C. X., Xie, S. R., Song, Z. L., Xia, S. P., and Strm, M. E. (2021). Biogeochemical cycling of iron (hydr-)oxides and its impact on organic carbon turnover in coastal wetlands: a global synthesis and perspective. *Earth Sci. Rev.* 218:103658. doi: 10.1016/j.earscirev.2021.103658

Yu, L., Zhuang, T., Bai, J. H., Wang, J. J., Yua, Z. B., Wanga, X., et al. (2019). Effects of water and salinity on soil labile organic carbon in estuarine wetlands of the Yellow River Delta. China. *Ecohydrol. Hydrobiol.* 20, 556–569. doi: 10.1016/j.ecohyd.2019.12.002

Zhai, Y. M., Hou, M. M., and Nie, S. A. (2018). Variance of microbial composition and structure and relation with soil properties in rhizospheric and non-rhizospheric soil of a flooded paddy. *Paddy Water Environ.* 16, 163–172. doi: 10.1007/s10333-017-0627-6

Zhang, G. S., Liu, H. J., Liu, R. P., and Qu, J. H. (2009). Removal of phosphate from water by a Fe-Mn binary oxide adsorbent. *J. Colloid Interface Sci.* 335, 168–174. doi: 10.1016/j.jcis.2009.03.019

Zhang, H. X., Zheng, S. L., Ding, J. W., Wang, O. M., and Liu, F. H. (2017). Spatial variation in bacterial community in natural wetland-river-sea ecosystems. *J. Basic Microbiol.* 57, 536–546. doi: 10.1002/jobm.201700041

Zhang, X. W., Kong, L. W., Cui, X. L., and Yin, S. (2016). Occurrence characteristics of free iron oxides in soil microstructure: evidence from XRD. SEM and EDS. *Bull. Eng. Geol. Environ.* 75, 1493–1503. doi: 10.1007/s10064-015-0781-2

Zhang, Y., Liu, X. L., Fu, C. Y., Li, X. H., Yan, B. X., and Shi, T. H. (2019). Effect of Fe^{2+} addition on chemical oxygen demand and nitrogen removal in horizontal subsurface flow constructed wetlands. *Chemosphere* 220, 259–265. doi: 10.1016/j.chemosphere.2018.12.144

Zhang, Z. W., Zhu, Z. X., Fu, W. L., and Wen, Z. L. (2012). Morphology of soil iron oxides and its correlation with soil-forming process and forming conditions in a karst mountain. *Environ. Sci.* 33, 2013–2020. doi: 10.13227/j.hjkx.2012.06.014

Zhang, Z. X., Yang, K. Y., Wang, P., and Gao, Y. (2001). A study on the availability of Fe in the dry farming yellow moist soil. *Soil Fertilizer* 2001, 27–30.

Zhang, Z. Y., and Furman, A. (2021). Soil redox dynamics under dynamic hydrologic regimes - a review. *Sci. Total Environ.* 763:143026. doi: 10.1016/j.scitotenv.2020.143026

Zhao, Q., Adhikari, D., Huang, R. X., Patel, A., Wang, X. L., Tang, Y. Z., et al. (2017). Coupled dynamics of iron and iron-bound organic carbon in forest soils during anaerobic reduction. *Chem. Geol.* 464, 118–126. doi: 10.1016/j.chemgeo.2016.12.014

Zhao, Z. J., Jin, R., Fang, D., Wang, H., Dong, Y., Xu, R. K., et al. (2018). Paddy cultivation significantly alters the forms and contents of Fe oxides in an Oxisol and increases phosphate mobility. *Soil Tillage Res.* 184, 176–180. doi: 10.1016/j.still.2018.07.012

Zhao, Z. M., Zhang, X., Cheng, M. Q., Song, X. S., Zhang, Y. J., and Zhong, X. M. (2019). Influences of iron compounds on microbial diversity and improvements in organic C. N, and P removal performances in constructed wetlands. *Microbial Ecol.* 78, 792–803. doi: 10.1007/s00248-019-01379-7

Zhou, J. M., and Shen, R. F. (2013). *Dictionary of Soil Science*. Beijing: Science Press.

Zou, Y. C., Jiang, M., Yu, X. F., Lu, X. G., David, J. L., and Wu, H. T. (2011). Distribution and biological cycle of iron in freshwater peatlands of Sanjiang Plain. Northeast China. *Geoderma* 164, 238–248. doi: 10.1016/j.geoderma.2011.06.017